One-Dimensional Zigzag Chains of Cs^-: The Structures and Properties of Li^+(Cryptand[2.1.1])Cs^- and Cs^+(Cryptand[2.2.2])Cs^-

Andrew S. Ichimura,*,‡ Rui H. Huang,† Qingshan Xie,† Philip Morganelli,‡ Amy Burns,† and James L. Dye*,†

Department of Chemistry, Michigan State University, East Lansing, Michigan 48824, and Department of Chemistry and Biochemistry, San Francisco State University, 1600 Holloway Avenue, San Francisco, California 94132

Received: February 24, 2006; In Final Form: April 29, 2006

The crystal structure and properties of lithium (cryptand[2.1.1]) ceside, Li^+(C211)Cs^-, are reported. Li^+(C211)Cs^- is the second ceside and third alkalide with a one-dimensional (1D) zigzag chain of alkali metal anions. The distance between adjacent Cs^- anions, 6 Å, is shorter than the sum of the van der Waals radii, 7 Å. Optical, magic angle spinning NMR, two-probe alternating and direct current conductivity, and electron paramagnetic resonance measurements reveal unique physical properties that result from the overlap of adjacent Cs^- wave functions in the chain structure. The properties of cesium (cryptand[2.2.2]) ceside, Cs^+(C222)Cs^-, were also studied to compare the effects of the subtle geometric changes between the two 1D zigzag chain structures. Li^+(C211)Cs^- and Cs^+(C222)Cs^- are both low-band-gap semiconductors with anisotropic reflectivities and large paramagnetic ^{133}Cs NMR chemical shifts relative to Cs^-(g). An electronic structure model consistent with the experimental data has sp^2-hybridized Cs^- within the chain and sp-hybridized chain ends. Ab initio multiconfiguration self-consistent field calculations on the ceside trimer, Cs_3^{3-}, support this model and indicate a net bonding interaction between nearest neighbors. The buildup of electron density between adjacent Cs^- anions is visualized through an electron density difference map constructed by subtracting the density of three cesium atoms from the short Cs_3^{3-} fragment.

Introduction

Alkalides are a unique class of ionic salts that have alkali metal anions (where M^- is Na^-, K^-, Rb^-, or Cs^-) as the negative ions and alkali cations embedded in cryptands, crown ethers, or their aza analogues as the positive counterions.[1−8] Coulombic attraction between the complexed cations and M^- anions stabilizes the salt, but we would expect Coulomb repulsion between the anions to keep them separated from one another. Yet, of the 37 published alkalide crystal structures, five have alkali metal anions in close proximity at distances smaller than the sum of the van der Waals radii.[9] Two salts, K^+(C222)K^- (where C222 is cryptand[2.2.2], Chart 1) and Rb^+(C222)Rb^- have very similar structures with pairs of anions surrounded by complexed cations. In addition, the structure of the first sodide dimer, Na_2^{2-}, was recently reported.[10] Even more remarkable are the salts Rb^+(18-crown-6)Rb^- and Cs^+(C222)Cs^-, in which linear chains of Rb^- and Cs^-, respectively, are found.[9,11] Low-dimensional nanoscale materials are currently receiving considerable experimental and theoretical attention, and the existence of these one-dimensional (1D) systems of alkali metal anions raises pertinent questions about their properties and electronic structures.

In the present work, we report the synthesis, crystal structure, and properties of a new compound, Li^+(cryptand[2.1.1])Cs^- (abbreviated Li^+(C211)Cs^-), which is the second ceside and the third alkalide that has a linear zigzag chain of alkali metal anions. Although the structure and some properties of Cs^+(cryptand[2.2.2])Cs^- (abbreviated Cs^+(C222)Cs^-), have been previously reported,[11,12] we include here a number of new measurements and interpretations. From a materials science perspective, these two cesides are intriguing because they contain the largest monatomic anion, Cs^-, which should be highly polarizable, and a complexed cation that balances the negative charge. The Herzfeld criterion for metallization relates the static polarizability, R, to the molar volume, V, through $4\pi N\alpha_0/3V = R/V$ and states that if this ratio is greater than one, then the substance will be metallic.[13,14] Part of the impetus for synthesizing Li^+(C211)Cs^- was to probe the Herzfeld criterion with a novel material. To this end, the temperature-dependent powder resistivities of both cesides were measured.

CHART 1

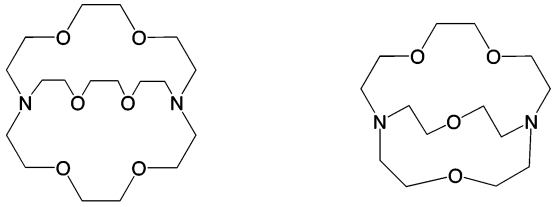

The primary diagnostic for alkali metal anions is the NMR chemical shift.[12] The closed-shell ns^2 electron configuration diamagnetically shields the nucleus and results in a substantial upfield resonance. For example, the chemical shift of Na^- is at −60 to −65 ppm relative to Na^+(aq), both in solution and in the solid state.[15] The chemical shifts of the larger anions, Rb^-, Cs^-, and to a lesser extent K^-, are more sensitive measures of

* Authors to whom correspondence should be addressed. E-mail: dye@msu.edu; ichimura@sfsu.edu.
† Michigan State University.
‡ San Francisco State University.

10.1021/jp061200l CCC: $33.50
Published on Web 06/02/2006

environmental effects, such as the solvent dieletric constant, concentration in solution, temperature, and the local surroundings within a crystal. Nevertheless their large negative chemical shifts (relative to the cation at infinite dilution) permit identification of the alkali anion. The proximity of alkali anions in the solids that have dimers and chains results in large Ramsey shifts[16] of their NMR resonances relative to M^- in dilute solutions or in structures that have isolated anions.[10,12,17] Note that the complexed cations also have substantial Ramsey NMR chemical shifts, but these are much less sensitive to their environment because they are sequestered inside complexant molecules.

The optical absorbance spectrum of $Cs^+(C222)Cs^-$ thin films was first reported in 1979[18] and was unusual for an alkalide because at least three peaks were observed. In the more typical case where an alkalide is in a nearly isotropic environment, a single peak ascribed to the *n*s-to-*n*p transition is observed. At the time, the structure of $Cs^+(C222)Cs^-$ had not been determined. With the current insight gained from the crystal structure, it is known that the 1D chain provides an anisotropic environment about Cs^- such that the degeneracy of the p-orbitals should be lifted. From this perspective, multiple absorptions might be expected. In both $Li^+(C211)Cs^-$ and $Cs^+(C222)Cs^-$, the question of optical anisotropy may be answered by single-crystal reflectance spectroscopy using plane-polarized light as was done for $Na^+(C222)Na^-$.[19]

The electronic structure of potasside dimers, K_2^{2-}, was studied by ab initio calculations.[20] A valence bond interpretation accounted for the stability of the anion dimers by placing two of the electrons in a σ-bond between each K^- and the other two electrons in localized nonbonding sp-hybrid orbitals that point away from the nuclei along the internuclear axis toward the point positive charges required for stability of the dimer. Although this view is oversimplified by neglect of the effect of the position of the complexed cations, the model provides a convenient physical picture to understand the stability of K_2^{2-} despite the Coulomb repulsion between anions. In the present work, the preliminary results of multiconfiguration self-consistent field (MCSCF) calculations for Cs^- trimers, Cs_3^{3-}, are reported.

To derive meaningful comparisons between $Li^+(C211)Cs^-$ and $Cs^+(C222)Cs^-$, fresh samples of the latter compound were prepared and characterized. The full suite of experimental methods included X-ray diffraction, single-crystal reflectance and thin film absorbance spectroscopy, differential scanning calorimetry (DSC), electron paramagnetic resonance (EPR), ^{133}Cs and ^{7}Li magic angle spinning nuclear magnetic resonance (MAS-NMR), magnetic susceptibility, and direct current (DC) conductivity measurements. These experiments in conjunction with ab initio computations permit insight into the intrinsic properties and the nature of defects in ceside chains.

Experimental Methods

Synthesis. Cryptand[2.1.1] and cryptand[2.2.2] were purchased from Aldrich and purified by sublimation. Lithium was purchased from AESAR and used as received. Cesium metal was a gift from the Dow Chemical Co.

The synthesis of $Li^+(C211)Cs^-$ proceeded as follows: 1.4 mmol of lithium and C211 were placed on one side of a two-chambered K-cell,[4,21] and 1.4 mmol of cesium was placed in a sidearm on the opposite side. The cesium was distilled to form a mirror, and the sidearm was sealed off from the K-cell. Methylamine was distilled onto the lithium metal and C211 at −70 °C. After all lithium metal and C211 had been dissolved, the dark blue solution was poured through a frit onto the cesium mirror. The methylamine was removed under vacuum overnight and then dimethyl ether was added and pumped away to remove lingering methylamine. Approximately 25 mL of fresh dimethyl ether was added and the solid was dissolved at −78 °C. To form a saturated solution of the ceside, diethyl ether was added and then some dimethyl ether was removed. Crystals up to 2 cm in length were grown by slowly removing the majority of the primary solvent over a period of 2 days at −78 °C. $Cs^+(C222)Cs^-$ was prepared according to a previously published method.[21] The crystal structure was determined with a Bruker CCD diffractometer and low-temperature accessory.

The $Li^+(C211)Cs^-$ crystals were kept at or near liquid nitrogen temperature under vacuum or a dry nitrogen atmosphere at all times during transfer to sample holders. Fresh red-gold, gold, and black crystals were placed in a mortar precooled to 77 K in a nitrogen-purged glovebag. At this stage, the crystals were hand-sorted by color. The majority of the crystals were red-gold while some gold crystals and a few small black crystals were obtained. The red-gold and gold crystals were crushed with a cold pestle and placed in the appropriate sample holders at 77 K for solid-state MAS-NMR, EPR, DSC, magnetic susceptibility, and DC conductivity measurements. Magic angle spinning NMR, DSC, and conductivity samples were run immediately, but the powder EPR samples were sealed off under vacuum and stored at 77 K until measured.

Magic Angle Spinning NMR. Crushed red-gold crystals and intact black crystals were loaded into separate ZrO_2 rotors and placed into liquid nitrogen. The NMR cryostat was cooled to −70 °C, and the samples were transferred rapidly to the probe. The sample spin rate was changed to ensure correct identification of the isotropic chemical shift. A Varian VXR 400S spectrometer was used to acquire ^{7}Li and ^{133}Cs MAS-NMR spectra.

Differential Scanning Calorimetry. A small amount of crushed crystals was placed in an aluminum pan, covered with an aluminum lid, and loaded into the sample press. The sample holders and press were kept in contact with liquid nitrogen in a glovebag to prevent thermal decomposition of the alkalide. The low-temperature accessory of the Shimadzu DSC-50 calorimeter was used to measure thermal data from −80 to 50 °C.

Two-Probe Direct Current Conductivity and Alternating Current Impedance Spectroscopy. The two-probe conductivity cell has two gold-coated electrodes, one fixed in position and one that is spring-loaded. The sample diameter is 2 mm, and the final height was 3 mm. Before the ceside powder was packed into the cell, the tips of the gold electrodes were coated with a small quantity of potassium metal to ensure good electrical contact. This has the added benefit that electrode effects, such as the formation of a Schottky barrier at the probe−sample junction, are minimized.[22] For the two-probe impedance measurements, the frequency was stepped logarithmically between 5 Hz and 11.7 MHz at voltages between 50 mV and 1 V. A Hewlett-Packard 4192A low-frequency impedance analyzer interfaced to the LabView program was utilized for impedance measurements. For DC measurements, the conductivity cell was interfaced to a Keithley electrometer via LabView, and the current was measured with a ±0.1 V bias as a function of temperature.

Electron Paramagnetic Resonance. Individual gold, red-gold, and black $Li^+(C211)Cs^-$ single crystals were placed in separate 4 mm o.d. quartz tubes and sealed off under vacuum. The preparation of powdered ceside EPR samples was described above. Spectra were recorded with a Bruker ESP300E spec-

TABLE 1: Crystallographic Data for Li^+(Cryptand[2.1.1])Cs^-

cell parameters	$a = 23.748(15)$ $b = 13.434(8)$ $c = 8.212(12)$ $\beta = 75.34(9)°$ $V = 2534.6(43)$ Å^3
temperature	173 K
space group	monoclinic, $C2/m$
Z	4
number of unique reflections:	1752
number of parameters:	106
R for reflections with $I > 2\sigma$	0.120
R for all reflections	0.167

trometer, and the temperature was controlled with an Oxford Instruments 900E liquid helium cryostat or a Bruker VT2000 nitrogen gas flow cryostat.

Optical Spectra of Crystals and Thin Films. Single crystals of freshly prepared Li^+(C211)Cs^- and Cs^+(C222)Cs^- were transferred into a quartz optical cell (1 cm path length) that was attached directly to the synthesis vessel (K-cell). The optical cell was sealed off under vacuum at −78 °C thus ensuring that the surface of the crystals would remain pristine. The optical cell was kept cold during specular reflectance measurements by placing the optical cell in direct contact with a cold copper block (∼−70 to −40 °C) that was mounted on a 3D translational stage and cooling with a stream of cold nitrogen gas in a nitrogen-purged glovebag. The Cassegrainian optics for reflectance studies were also kept in the glovebag, and light was passed to a Guided Wave model 260 spectrophotometer via optical fibers. For these studies, crystals were chosen based on their overall reflecting ability to increase the signal-to-noise ratio. Because of the geometry of the crystals only a single face could be studied, and the Miller indices were unknown. In addition, because of instrument limitations, the crystal was rotated rather than the plane of polarization. Ceside thin films were prepared by flash evaporation of a dimethyl ether solution, in which a few small, freshly prepared red-gold crystals were dissolved in approximately 1 mL of solvent. The solution was poured into a 1 cm path length quartz cell, and the temperature was raised to about −35 °C. The larger bulb of the optical cell was then immersed in liquid nitrogen, which caused solvent evaporation and thin film formation in a matter of seconds. This optical cell was then placed in a stream of cold N_2 gas in a home-built quartz dewar, and absorbance spectra were recorded.

Results and Discussion

Li^+(Cyptand[2.1.1]Cs^- Crystal Structure and Diagrams. Two types of crystals were formed in one preparation, elongated rectangular gold and red-gold crystals and small blocky black crystals. The structure of the gold crystals was determined. The gold and red crystals differ mainly in the number of defect centers, vide infra. The crystal system is monoclinic with space group $C2/m$ (No. 12). The cell parameters are listed in Table 1, and the CIF file is given in the Supporting Information.

The striking feature of the crystal structure, Figure 1A, is that like charges get together to form zigzag chains of cesium anions with a center-to-center distance of 6.0 Å. This is remarkable because the van der Waals radius of Cs^- in crystal structures that have isolated ceside anions, such as Cs^+(18-crown-6)$_2Cs^-$,[9] in which each anion is surrounded by complexed cations, is 3.5 Å. Therefore, in Li^+(C211)Cs^-, adjacent cesium anions overlap by approximately 1.0 Å. The angle between three adjacent Cs^- ions is 86.7°. This is the third alkalide crystal structure to have linear chains of M^-. Cs^+(C222)Cs^- has a similar Cs^- chain structure in which the distance between pairs of anions is 6.38 Å and the angle between three neighbors is 118.0°.[11] In Rb^+(18-crown-6)Rb^-, the Rb^--to-Rb^- distance is 5.13 Å, the same as that in rubidide pairs in Rb^+(C222)Rb^-.[9]

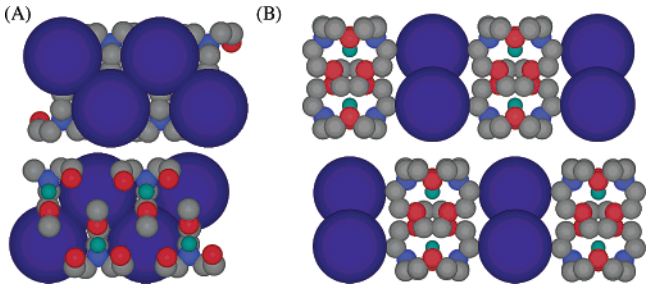

Figure 1. Ion and atom packing in Li^+(C211)Cs^-: (A) perpendicular to the chains; (B) a view down the chains. Cs, Li, N, O, and C atoms are purple, green, blue, red, and gray, respectively.

From the standpoint of cell type and parameters, the ceside crystal structure resembles that of Li^+(cryptand[2.2.1])e^-.[23] In this electride, the trapped electrons form 1D antiferromagnetically coupled chains, and the arrangement of complexed cations relative to the electrons strongly resembles the cation−anion placement in the ceside, Figure 1B. The encapsulated Li^+ fragment of the ceside salt is typical of other alkalide salts and the electride that contains the Li^+(cryptand[2.1.1]) cation. Oxygen and tertiary nitrogen atoms of the complexant point inward stabilizing Li^+ in a hexacoordinate arrangement. Stabilizing charge balance for the anionic chain is provided by interleaved complexed cations that form their own 1D zigzag arrays. The alternating arrays of positive and negative charge likely lead to the brittleness of the crystals, as they tend to fragment lengthwise when a mild force is applied.

The structure of the black crystals was not solved. However, they strongly resemble Li^+(cryptand[2.1.1])e^- in appearance. The black color is generally associated with a high concentration of defect electrons. The solid-state NMR and EPR spectra of this form of "doped" ceside provide useful information about the nature of chain-end and electron defects in alkali metal anion chains.

Magic Angle Spinning NMR. The ^{133}Cs MAS-NMR spectrum of crushed gold-red Li^+(C211)Cs^- crystals yields a temperature-independent ^{133}Cs chemical shift of +72.6 ppm (Figure 2a**)**. The chemical shift of Cs^- in crystalline Cs^+(C222)Cs^- is even larger at +127.4 ppm (Figure 2b**)**. In a previous publication,[12] the peak at 127.4 ppm was interpreted as an "exclusive" complex of Cs^+ with cryptand[2.2.2], that is, one in which Cs^+ was complexed by C222 in the manner of a crown ether rather than a cryptand. In this work, optical spectra in combination with the NMR data show conclusively that this peak is due to a large downfield shift of Cs^- relative to Cs^-(g). Relative to the isolated Cs^- in Cs^+(18-crown-6)$_2Cs^-$ (−213 ppm),[12] these values represent overall paramagnetic shifts of +285.6 and +340.4 ppm for the Cs^- anion in Li^+(C211)Cs^- and Cs^+(C222)Cs^-, respectively. The inclusive complex of the cesium cation, Cs^+(cryptand[2.2.2]), experiences a large Ramsey shift of +238.3 ppm, which is typical for Cs^+ sequestered inside this complexant.[24] In previous work,[25] it was found that the quadrupole coupling of the cation is large so that only the central transition shows, while that of the cesium anion is small and results in all transitions being involved. This accounts for the larger magnitude and anisotropy of the NMR spectrum of the anion.

The lithium cation complexed by cryptand[2.1.1] in gold crystals of Li^+(C211)Cs^- has a small temperature-independent

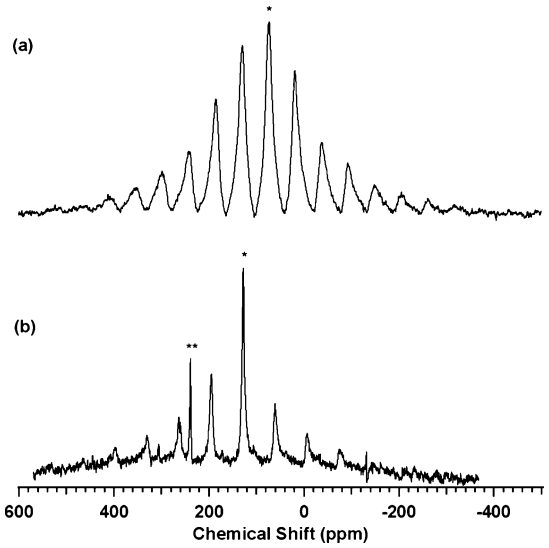

Figure 2. ^{133}Cs MAS-NMR spectra of (a) $Li^+(C211)Cs^-$ and (b) $Cs^+(C222)Cs^-$. A single dot signifies the assignment to Cs^-. Two dots identify the peak of complexed Cs^+. Others are spinning sidebands.

chemical shift of −2.1 ppm relative to the value of $^7Li^+$ at infinite dilution. This behavior is typical for the $Li^+(C211)$ complex in other alkalides, such as $Li^+(C211)Na^-$ and Li^+-(C211) in solutions. Quite the opposite behavior was observed for the strongly temperature-dependent ^{7}Li chemical shift of the black crystals. This chemical shift, extrapolated to high temperatures ($1/T = 0$) yields $\sigma(\infty) = -0.3 \pm 3$ ppm, which is comparable to that of Li^+(cryptand[2.1.1]) complexes in solution. At 233 K, the ^{7}Li chemical shift for the black crystals was +20 ppm relative to $Li^+(aq,\infty)$, which is approximately one-third of the value for Li^+ in the electride, $Li^+(C211)e^-$.[23] The electride has one electron per complexed cation and has a ^{7}Li chemical shift of 57 ppm at 233 K. Since $Li^+(C211)Cs^-$ has one-third of this value, it suggests that there is on average one-third of an electron per Li^+, a very high concentration of electrons in an alkalide. These small blocky black crystals of $Li^+(C211)Cs^-$ did not exhibit a ^{133}Cs resonance, probably due to paramagnetic broadening by the unpaired electrons. Such paramagnetic broadening into the baseline has been seen for cesium in a zeolite.[26]

Magnetic susceptibility measurements on crushed crystals show that both cesides have low paramagnetic defect concentrations. The susceptibility accounted for <1% and ∼1% defects per mole of ceside for $Li^+(C211)Cs^-$ and $Cs^+(C222)Cs^-$, respectively. Such low defect concentrations are typical for alkalide preparations and are not large enough to significantly affect the isotropic chemical shift, since separate sample preparations yield the same chemical shift but different defect concentrations. The most common defects in alkalides result from electrons trapped in anion vacancies. In the case of the 1D ceside chains, however, EPR studies show that defect electrons comprise a small fraction of the paramagnetic impurities. Hence, the ^{133}Cs paramagnetic shift observed in the MAS-NMR studies requires an alternative explanation.

Differential Scanning Calorimetry. Alkalides and electrides typically decompose under vacuum at elevated temperatures by reductive cleavage of the complexant's C−O bonds. $Li^+(C211)Cs^-$ was observed to form a dark blue liquid as the crystalline residue in the K-cell approached ambient temperature. Differential scanning calorimetry measurements were performed on separate samples of the gold and red-gold crystals. Gold crystals show a small endothermic transition at +13 °C signaling the onset of melting (Figure 3). A large exotherm associated with decomposition of the complexant followed immediately thereafter. The thermal behavior of the red crystals depended on the crystal chosen. Bright red crystals exhibited a heating profile identical to that of the gold ones, but those with a dark red color had an exotherm that preceded melting with an onset temperature of ∼−15 °C. Electron paramagnetic resonance measurements show that the red-gold crystals have a higher concentration of electron defects than the gold ones. Since typical defects in alkalides are trapped electrons, the first exotherm can reasonably be assigned to the reaction of these defects with the complexant. The gold crystals have very low concentrations of defect electrons and do not exhibit the premelt exotherm. The thermal behavior of the black crystals was qualitatively different from the elongated gold and red crystals. In multiple runs, the black crystals did not melt as the temperature was increased but simply decomposed at temperatures above −15 °C. The gold crystals have reasonable thermal stability in line with other alkalides, but they are clearly not room-temperature stable as are alkalides prepared from azacryptands.[7]

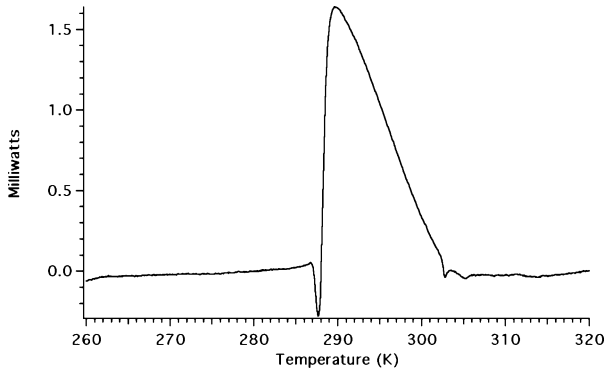

Figure 3. Differential scanning calorimetry trace of crushed gold crystals of $Li^+(C211)Cs^-$.

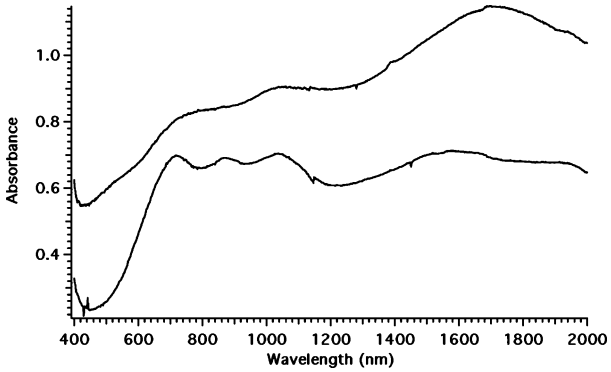

Figure 4. Thin film absorbance spectra of $Li^+(C211)Cs^-$ (top) and $Cs^+(C222)Cs^-$ (bottom).

Absorption and Reflectance Spectroscopy. The absorption spectra of $Li^+(C211)Cs^-$ and $Cs^+(C222)Cs^-$ thin films are shown in Figure 4. Multiple absorption bands are observed in the visible and near-infrared (NIR) regions of the spectrum (Table 2). There are two striking features of these spectra that are in sharp contrast to the spectra of other alkalides.

Typical absorption or reflectance spectra of alkalides have a single broad absorption band that tends to be characteristic of a particular nucleus. For example, the absorption bands of Na^-, K^-, Rb^-, and Cs^- in thin films occur at or near 650, 810, 890, and 950 nm, respectively.[24] However, there are two and three peaks for $Li^+(C211)Cs^-$ and $Cs^+(C222)Cs^-$, respectively, in the 400−1100 nm region. When the alkalide environment is

TABLE 2: Absorbance and Reflectance Optical Bands (in nm) of $Li^+(C211)Cs^-$ and $Cs^+(C222)Cs^-$

	thin film (absorbance)	crystal (reflectance)
$Li^+(C211)Cs^-$	770 (sh), 1042, 1640	822 (sh), 1070 (sh), 1710
$Cs^+(C222)Cs^-$	720, 876, 1038, 1581	633, 827, 1120, broad rise[a] 678, 827 (sh), 1076, ~1600[b]

[a] Starting orientation. [b] ~90° turn.

spatially isotropic or nearly so, degenerate or nearly degenerate p-states would result, and thus a single observable metal-dependent s-to-p-type transition in the 400−1100 nm region should be observed. The crystal structures of both linear-chain cesides show that the environment about each metal center is highly anisotropic due to the proximity of neighboring Cs^- ions. Under these circumstances, the degeneracy of the p-states is lifted so that the s-to-p transition can yield two or three distinct transitions, some of which are shifted to higher energies than previously observed for cesides in solution or the solid state. A similar observation was made for the Na_2^{2-} dimer that was reported recently.[10] The thin film absorbance spectrum of this sodide had two peaks, one blue-shifted to 480 nm and the other at the more typical value of 648 nm. Despite the structurally induced differences in the optical spectra, optical and solid-state NMR spectroscopy confirm the presence of alkali metal anions in these solids.

The second major difference in the thin film spectra of $Li^+(C211)Cs^-$ and $Cs^+(C222)Cs^-$ from those of other alkalides is that the NIR band from 1100 to 2000 nm is very intense. In previous work, thin films of the alkalides K^-, Rb^-, and Cs^- prepared by flash evaporation from ammonia solutions that contain cryptands have NIR shoulders or bands that tend to increase in intensity as one goes from K to Cs.[27,28] It was postulated that the NIR band was due in part to trapped electrons but that some fraction of the band was associated with a plasma edge indicative of delocalized electron states. However, ammonia does not support alkalide formation, and the complexation constant of the alkali cation may be less in ammonia compared to ethers or primary amines. Therefore, a percentage of trapped electrons might be expected (and was observed) after rapid solvent evaporation, even for Na metal, which has been notoriously resistant to electride formation until recently.[29] In the present work the primary solvent dimethyl ether was used to prepare the films under conditions that should favor alkalide formation. To discriminate between the broad absorption band that would occur by trapped electron accumulation and that due to a plasmalike resonance of intrinsic conduction electrons, reflectance studies were carried out on single crystals of both cesides. Electron paramagnetic resonance studies (vide infra) show that the electron concentration in such crystals is far too low to contribute a significant IR band.

Figures 5a and 5b show plane-polarized reflectance spectra for single crystals of $Li^+(C211)Cs^-$ and $Cs^+(C222)Cs^-$, respectively. Peak positions are listed in Table 2. A quick comparison between the thin film and the single-crystal reflectance spectra shows that the same optical bands are present in both sampling arrangements. This is a particularly important observation because it gives credence to the method of flash evaporation for preparing alkalide (or electride) films that retain the principal spectroscopic features of the crystal, even for complex spectra such as those shown. In other words, interpretations that can be drawn from structurally intact crystals may also be inferred from thin films, which are much easier to prepare.

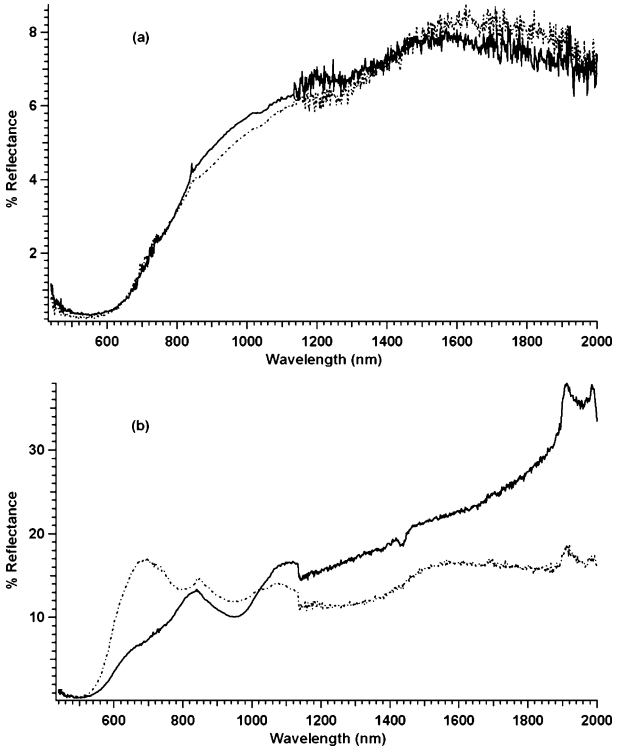

Figure 5. Single-crystal reflectance spectra of (a) $Li^+(C211)Cs^-$ and (b) $Cs^+(C222)Cs^-$ taken with plane-polarized light. Dashed lines represent crystal rotation by (a) 45° and (b) 90°, respectively.

Four distinct electronic transitions are observed in both orientations of $Cs^+(C222)Cs^-$. Three bands in the vis−NIR have small wavelength shifts but significant intensity changes at different orientations, while the broad NIR band continues to rise in one orientation and remains relatively constant out to 2000 nm in the other. The sharp resonances at 1700 and 1900 nm in the spectra of $Cs^+(C222)Cs^-$ are ascribed to CH stretching overtone and combination bands of the cryptand. The single-crystal reflectance spectra of $Li^+(C211)Cs^-$ have shoulders where peaks were located in the thin film spectrum, in addition to the same broad NIR band with a slightly red-shifted peak at 1710 nm. For the particular crystal face of $Li^+(C211)Cs^-$ available for study, the change in orientation upon rotation proved to be a minor perturbation. The thin flat crystals prevented studies at other orientations. The changes in intensity and peak position of the plane-polarized reflectance spectra of both cesides upon crystal rotation provide confirmation that the optical spectra of ceside chains are anisotropic.

A typical alkalide preparation leads to the inclusion of, at most, a few percent trapped electron defects, too low to produce a NIR band in transmission or reflection spectroscopy. Thus, the NIR band of both cesides studied in this work is too intense to be accounted for solely on the basis of trapped electrons. This suggests that the electronic transition in question arises from inter- and/or intraband transitions, with the implication that ceside chains may be low-dimensional conductors or semiconductors. A related solid, $K^+(C222)e^-$, is nearly metallic and also exhibits a plasma absorption in the NIR.[30,31] The plasma absorption is directly related to the conductivity of this solid, which arises mainly from defect electrons and is best described by a random hopping or percolation mechanism. To gain insight into the nature of the ceside NIR band, two-probe DC conductance and alternating current (AC) impedance measurements were performed on crushed ceside crystals.

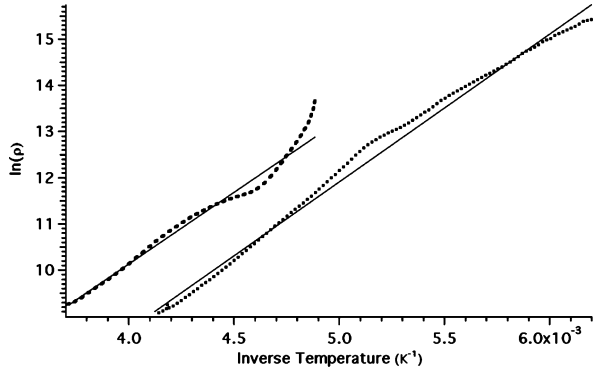

Figure 6. Two-Probe DC conductivity vs temperature measurements on crushed crystals of $Li^+(C211)Cs^-$ (dotted line) and $Cs^+(C222)Cs^-$ (dashed line).

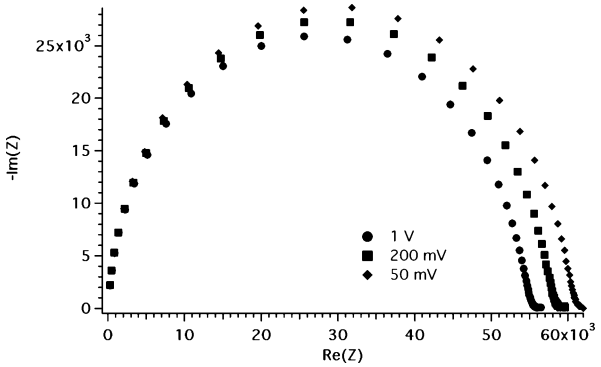

Figure 7. AC impedance spectra for $Li^+(C211)Cs^-$ crushed crystals at 226 K.

Direct Current Conductivity and Alternating Current Impedance. The conductivity of packed powders of each ceside was studied as a function of temperature. The data were converted to resistivity, and plots of ln(ρ) versus reciprocal temperature for both cesides are shown in Figure 6. In addition, AC impedance measurements were carried out on $Li^+(C211)Cs^-$, Figure 7, and demonstrate that good electrical contact was made with the sample. The voltage dependence was minor implying nearly ohmic behavior. The resistivity (in Ω cm) was found to vary over 3 orders of magnitude for $Li^+(C211)Cs^-$, from a high of 4×10^6 at 161 K to a low of about 8×10^3 at 245 K. The resistivity of $Cs^+(C222)Cs^-$ varied over 2 orders of magnitude from 8.1×10^5 at 205 K to 1.1×10^4 at 282 K. The best fit to these data was based on the thermal population of a conduction band, with band gaps of 0.55 and 0.53 eV for $Li^+(C211)Cs^-$ and $Cs^+(C222)Cs^-$, respectively. The fit to a random 1D, 2D, or 3D hopping model was poor. However, because of the substantial temperature dependence of the resistivity and the marked deviations from linearity at the lower temperatures, it is likely that charge transport operates by a different mechanism at low temperatures. At higher temperatures, the cesides apparently behave as low-band-gap semiconductors, an interpretation consistent with the reflectance spectra. The plasma edge should lie just outside our spectrometer's range. However, this interpretation must be applied with caution. Typical alkalides are diamagnetic and insulating, but much higher conductivities can be realized by the purposeful introduction of defects. It was found that doping $Cs^+(18C6)_2e^-$ with ceside produced a solid with orders of magnitude greater conductivity than the pure electride.[22] Additionally, powder conductivity studies of $K^+(C222)e^-$ generally had higher conductivities than a single crystal.[30] Therefore, the introduction of defects, such as M^- or e^- generated by crushing crystals, can increase the conductivity. A definitive answer could be provided by conductivity measurements on high-quality/low-defect single crystals. This would have the additional advantage that the expected charge transport anisotropy could be readily detected. But, because the crystals of both cesides are very fragile, it was not possible to carry out single-crystal conductivity studies. Despite this shortcoming, the combination of powder conductivity and single-crystal reflectance measurements supports a model in which electrons thermally populate the conduction bands in these solids.

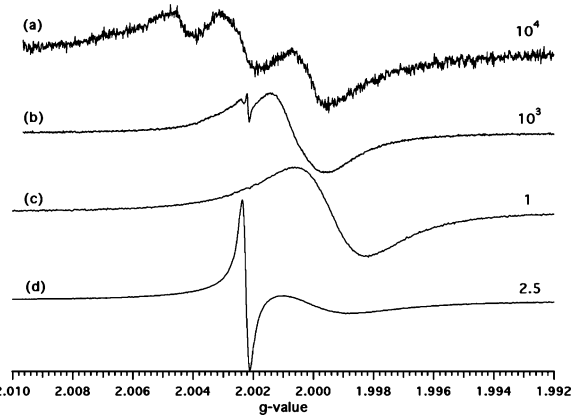

Figure 8. Electron paramagnetic resonance spectra of various colored single crystals of $Li^+(C211)Cs^-$ taken at 4 K: (a) gold, (b) red-gold, (c) black. Spectrum d is that of crushed gold crystals. Signal intensity is indicated by the relative gain to the right of each spectrum.

Electron Paramagnetic Resonance. The $6s^2$ electron configuration of Cs^- is closed-shell and should lead to a diamagnetic state in a perfect crystal. However, alkalides are always paramagnetic to some extent, and EPR studies reveal information on the nature of defect sites.[31,32] Figure 8 shows EPR spectra taken at 4 K plotted as a function of *g*-value for the three types of single crystals of $Li^+(C211)Cs^-$. Gold crystals (Figure 8a) have very few defect centers, and the spectrum is rather weak in intensity. The three-line pattern is orientation-dependent and there may be as few as two or as many as four resonances of varying intensity. This angular dependence is most likely associated with *g*-value anisotropy and corresponds to different trapping sites or perhaps crystallographically equivalent ones. ^{133}Cs ($I = {}^7/_2$) hyperfine anisotropy does not account for the spectrum since eight lines would be expected. In addition, if the NMR chemical shift of 419 ppm of the ceside relative to Cs^- in the gas phase (-346.4 ppm) were due entirely to Fermi contact or spin dipolar interactions, then the downfield shift would amount to a contact density of only 170 kHz or about 0.06 G. Such a perturbation is too small to yield the observed separation between resonances and would yield only a small increase in line width.

The EPR spectrum of red-gold crystals (Figure 8b) is much more intense than that of gold crystals. Rotation of the crystal with respect to the static field demonstrates an angular dependence of the broad signal ($\Delta H_{pp} = 3.0$ G) with a negative *g*-value shift, $g \approx 2.0007-2.0002$, and minor asymmetry of its line shape. The narrow EPR signal ($g = 2.00228$, $\Delta H_{pp} = 0.1$ G) has little or no angular dependence. Finally, the small blocky black crystals have very intense EPR spectra with a Lorentzian line shape ($\Delta H_{pp} = 3.0$ G) (Figure 8c). Their volume was approximately 1 mm^3 while the crystals with known structure were considerably larger, about 20 mm^3. The black crystals have a much higher density of spins. The *g*-value varies between 2.0007 and 1.9995 during crystal rotation in the static field. In addition, the temperature dependence of the EPR intensity

follows Curie Law behavior, consistent with magnetic susceptibility studies. Some of the black crystals also had a very small narrow signal at the free electron *g*-value. The characteristics of these single crystals yield a picture of the defect sites in this ceside, which is made more complete with the powder pattern spectrum of crushed red-gold and gold crystals.

To prepare a homogeneous sample for EPR that would minimize crystallite peaks, a mixture of red and gold crystals was ground to a fine powder in a liquid-nitrogen-cooled mortar and pestle. The resulting powder, though red-gold in color, was considerably darker than the parent crystals. The EPR spectrum is shown in Figure 8d and is well fit by the sum of two Lorentzian lines with different line widths and *g*-values. The narrow line ($\Delta H_{pp} = 0.38$ G, $g = 2.00228$) is characteristic of electrides and often seen in the EPR spectra of alkalides. This resonance is ascribed to trapped electrons in anion vacancies. The broad line has a substantial *g*-shift ($\Delta H_{pp} = 3.0$ G, $g = 2.0005$) and roughly indicates the average of the g-value extrema reported above for the red-gold crystals. The powder pattern spectrum is much more intense than the single crystals because crystal pulverization generated additional defects of both types at freshly exposed surfaces. In agreement with magnetic susceptibility measurements, the EPR signal intensity is inversely proportional to temperature over the range 4−260 K. The single-crystal and powder pattern EPR data in combination with the ^{7}Li and ^{133}Cs MAS-NMR spectra, suggest a possible model for defects in $Li^+(C211)Cs^-$ that differs from the aforementioned electron-occupied anion vacancies.

The negative *g*-shift of the broader $\Delta H_{pp} = 3.0$ G orientation-dependent and powder EPR signals indicates substantial spin−orbit coupling to cesium. Ab initio calculations, vide infra, show that the electronic structure of chain ends may be described as an unpaired electron in an sp-hybridized orbital of the terminal cesium anion. The substantial p-character supplies the requisite orbital angular momentum to account for the negative *g*-shift while s-character permits some contact density at the nucleus to broaden the EPR signal. Chain ends are therefore atom-localized paramagnetic centers in this ceside and are the primary defects based on the relative intensities of the lines in the single-crystal spectra.

According to this model, chain ends dominate the EPR spectrum of the small black single crystal. Ab initio calculations on the ceside trimer show that the singlet and triplet states are essentially degenerate in energy. An ensemble of chains of any length would obey the Curie Law as observed. Hence, the ^{7}Li NMR chemical shift of the black crystals was temperature-dependent. The high concentration of chain ends in the black crystals likely results in an exchange-narrowed signal accounting for the Lorentzian line shape.

Electron paramagnetic resonance can be used to measure charge transport properties provided that the particles have metallic or near-metallic conductivity. At X-band frequencies, however, the skin depth, which is a function of frequency and resistivity, is comparable to the crystal dimensions for $Li^+(C211)Cs^-$. Hence a Dysonian line shape indicative of conduction EPR was not expected or observed.

Electronic Structure of Cs_3^{3-}. To gain further insight into the electronic structure of zigzag ceside chains, MCSCF calculations were carried out on the ceside trimer, Cs_3^{3-}, using the Molpro suite of programs.[33] The Stuttgart relativistic small core pseudopotential basis set for cesium was modified to include diffuse and polarization functions to account for the highly polarizable metal anion and to recover a larger fraction of the electron correlation.[34] The final basis set consisted of

Figure 9. Electron density difference map of Cs_3^{3-} calculated at the CAS(6,6) level in which the cesium atom density was subtracted from the chain fragment.

CHART 2

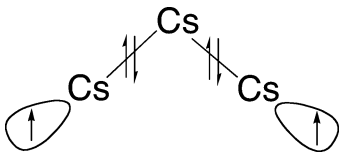

8s7p5d2f Gaussian functions contracted to 7s6p3d2f. All valence electrons and orbitals were correlated in the six-electron twelve-orbital (6,12) complete active space (CAS) MCSCF wave function. The geometry of the cesium trimer was fixed at the experimental atomic positions in $Li^+(C211)Cs^-$. Preliminary computations showed that Cs_3^{3-} was unbound relative to Cs_3^{2-} at the MCSCF level. Previous computational work on K_2^{2-} showed that charge balance, even at remote distances, was necessary to achieve bound anionic states. In the present work, point charges were placed at the 10 nearest neighbor cation positions that are closest to the trimer in accordance with the crystal structure. Each point carried 0.3 units of positive charge. The MCSCF computations with point charges show that the Cs_3^{3-} is bound (relative to Cs_3^{2-} plus an electron) by approximately 0.1 hartrees.

To gain physical insight into the possibility of bonding between nearest neighbor cesides, the electron density of the cesium atom at the MCSCF level was subtracted from Cs_3^{3-} at the atomic positions. The resulting electron density difference map (in the plane of the three Cs atoms) is shown in Figure 9. It is clear that electron density buildup between neighboring cesium anions implies bond formation, even at a distance of 6.0 Å. In addition, there is a commensurate depletion of charge on either side of the short chain. The valence bond picture that emerges from this analysis is shown in Chart 2. Four of the six valence electrons form bonds between cesium atoms. The remaining two electrons are essentially nonbonding and reside at the terminal atoms to maintain charge balance. In this picture, the central cesium becomes sp^2-hybridized while the terminal atoms have sp-hybridization.

The model is in accord with EPR measurements that identify atom-centered chain ends as the dominant defect in the ceside crystals. In $Li^+(C211)Cs^-$ and $Cs^+(C222)Cs^-$, the anions are in close proximity such that the distances between centers are 1.0 and 0.6 Å less than the sum of the van der Waals radii, respectively. The admixture of p-orbitals into the ground-state wave function results in bonding interactions between adjacent

Cs^- that help to stabilize the anionic chains and compensate for the energetic cost of the Coulombic repulsion.

In addition to accounting for the chain structure, the model provides a qualitative understanding of other experimental observations. Excluding chain ends, the bulk of the 1D zigzag arrays consists of diamagnetic centers, and according to powder conductivity measurements, the materials are semiconductors at best. Therefore, the ^{133}Cs NMR chemical shift does not have its origin in the Fermi contact interaction or Knight shift. As a result of sp-hybridization, however, the ^{133}Cs nuclei are deshielded relative to $Cs^-(g)$ resulting in the large Ramsey shift. Optical measurements of the ceside arrays have two or three transitions instead of one for cesides in spatially isotropic environments. Nondegenerate p-states are a natural consequence of the bent atomic arrangement, a situation that is likely to change the nature of the s-to-p transitions resulting in different energies. It is not possible to extrapolate the present model system to bulk properties, such as conductivity. However, due to the presence of vacant atomic π-orbitals perpendicular to the chain, we postulate that these orbitals form an energetically low-lying band that can be thermally populated with conduction electrons.

Several questions remain about the electronic structure of short oligomeric ceside chains, Cs_n^{n-}, $n > 3$, and the band structure of the bulk. Ab initio and density functional theory calculations that address these issues are in progress and will be reported in a subsequent paper.

Conclusions

Charge transport within alkalides and electrides usually involves defect centers in the crystal. For example, $K^+(C222)e^-$ is nearly metallic and has a 2D pore structure with anisotropic conductivity.[32] The conductivity in this solid most likely arises by a hole percolation mechanism since the temperature dependence is well fit by a random 2D hopping model. This points to an electron vacancy as one of the defects in this electride. The defects in $Li^+(C211)Cs^-$ are primarily localized electrons at chain ends with a very small percentage of defect electrons in anion vacancies. Although the EPR spectrum of $Cs^+(C222)Cs^-$ single crystals was not measured, based on the crystal structure it is reasonable to suppose that chain ends are also the main defects in this solid. Chain ends imply a ceside vacancy otherwise a diamagnetic state would result. The temperature dependence of the conductivity suggests that charge transport involves the thermal population of a conduction band rather than a hopping mechanism. In addition, the optical reflectance spectra indicate a plasmalike resonance at long wavelengths. From these data and an understanding of the defects in these solids, it is possible to conclude that the semiconducting behavior is an intrinsic property of the 1D ceside chains. Furthermore, because of the anisotropy in the single-crystal reflectance measurements, it is quite likely that charge transport would be anisotropic. According to our crushed crystal DC conductivity studies, these solids are on the $R/V < 1$ side of the Herzfeld criterion. Thus, they are nonmetals. However, to pin down the mechanism, verify transport directionality, and provide a better test of the Herzfeld inequality, single-crystal conductivity studies on high-quality gold crystals would be necessary.

The two cesides, $Li^+(C211)Cs^-$ and $Cs^+(C222)Cs^-$, differ in the angle and amount of overlap between adjacent centers. Nuclear magnetic resonance samples the local environment of the nuclei. It is hypothesized that the larger Ramsey shift of $Cs^+(C222)Cs^-$ compared to $Li^+(C211)Cs^-$ correlates with the bond angles, which are 118° and 86.7°, respectively. In this model, $Cs^+(C222)Cs^-$ has greater p-character that deshields the ^{133}Cs nucleus to a larger extent than in $Li^+(C211)Cs^-$. The distance between Cs^- may correlate with the conductivity, since $Cs^+(C222)Cs^-$ powders conduct less than $Li^+(C211)Cs^-$ at a given temperature. A larger distance decreases the overlap between p-orbitals on adjacent anions, and so more thermal energy is required to activate charge transport.

An electronic structure model that is consistent with the experimental data and supported by ab initio calculations has sp^2-hybridized Cs^- within the chain and sp-hybridized chain ends. As a result, $Li^+(C211)Cs^-$ and $Cs^+(C222)Cs^-$ have dramatically different properties from alkalide monomers (isolated M^-) and dimers, such as Na_2^{2-}. This study has revealed surprising details about 1D alkalide chains, but much experimental and theoretical work is needed to fully understand these materials.

Acknowledgment. This work was supported in part by the U. S. National Science Foundation under Grant No. DMR 9988881. The American Chemical Society Petroleum Research Fund Grant No. 38397-GB5 and Research Corporation Cottrell Science Award No. CC5646 also supported this work (A.S.I.).

Supporting Information Available: Crystallographic data and EPR spectra of single crystals of $Li^+(C211)Cs^-$. This material is available free of charge via the Internet at http://pubs.acs.org.

References and Notes

(1) Dye, J. L.; Ceraso, J. M.; Lok, M. T.; Barnett, B. L.; Tehan, F. J. *J. Am. Chem. Soc.* **1974**, *96*, 608−609.
(2) Tehan, F. J.; Barnett, B. L.; Dye, J. L. *J. Am. Chem. Soc.* **1974**, *96*, 7203−7208.
(3) Dye, J. L. *Sci. Am.* **1977**, *237*, 92−105.
(4) Dye, J. L. *Prog. Inorg. Chem.* **1984**, *32*, 327−441.
(5) Dye, J. L. *Chemtracts: Inorg. Chem.* **1993**, *5*, 243−270.
(6) Huang, R. H.; Huang, S. Z.; Dye, J. L. *J. Coord. Chem.* **1998**, *46*, 13−31.
(7) Kim, J.; Ichimura, A. S.; Huang, R. H.; Redko, M.; Phillips, R. C.; Jackson, J. E.; Dye, J. L. *J. Am. Chem. Soc.* **1999**, *121*, 10666−10667.
(8) Wagner, M. J.; Dye, J. L. In *Molecular Recognition: Receptors for Cationic Guests*, 1st ed.; Gokel, G. W., Ed.; Pergamon Press: Oxford, U. K., 1996; Vol. 1, pp 477−510.
(9) Huang, R. H.; Ward, D. L.; Dye, J. L. *J. Am. Chem. Soc.* **1989**, *111*, 5707−5708.
(10) Redko, M. Y.; Huang, R. H.; Jackson, J. E.; Harrison, J. F.; Dye, J. L. *J. Am. Chem. Soc.* **2003**, *125*, 2259−2263.
(11) Huang, R. H.; Ward, D. L.; Kuchenmeister, M. E.; Dye, J. L. *J. Am. Chem. Soc.* **1987**, *109*, 5561−5563.
(12) Dawes, S. B.; Ellaboudy, A. S.; Dye, J. L. *J. Am. Chem. Soc.* **1987**, *109*, 3508−3513.
(13) Herzfeld, K. F. *Phys. Rev.* **1927**, *29*, 701−705.
(14) Edwards, P. P.; Sienko, M. J. *Int. Rev. Phys. Chem.* **1983**, *3*, 83−137.
(15) Ellaboudy, A.; Dye, J. L. *J. Magn. Reson.* **1986**, *66*, 491−502.
(16) Ramsey, N. F. *Phys. Rev.* **1950**, *78*, 699−703.
(17) Kim, J.; Eglin, J. L.; Ellaboudy, A. S.; McMills, L. E. H.; Huang, S.; Dye, J. L. *J. Phys. Chem.* **1996**, *100*, 2885−2891.
(18) DaGue, M. G.; Landers, J. S.; Lewis, H. L.; Dye, J. L. *Chem. Phys. Lett.* **1979**, *66*, 169−172.
(19) Hendrickson, J. E.; Kuo, C. T.; Xie, Q.; Pratt, W. P., Jr.; Dye, J. L. *J. Phys. Chem.* **1996**, *100*, 3395−3401.
(20) Tientega, F.; Dye, J. L.; Harrison, J. F. *J. Am. Chem. Soc.* **1991**, *113*, 3206−3208.
(21) Dye, J. L. *J. Phys. Chem.* **1984**, *88*, 3842−3846.
(22) Moeggenborg, K. J.; Papaioannou, J.; Dye, J. L. *Chem. Mater.* **1991**, *3*, 514−520.
(23) Huang, R. H.; Wagner, M. J.; Gilbert, D. J.; Reidy-Cedergren, K. A.; Ward, D. L.; Faber, M. K.; Dye, J. L. *J. Am. Chem. Soc.* **1997**, *119*, 3765−3772.
(24) Dye, J. L.; DeBacker, M. G. *Annu. Rev. Phys. Chem.* **1987**, *38*, 271−301.

(25) Kim, J. Solid State Alkali Metal NMR Spectra and Magnetic Susceptibilities of Alkalides, Electrides and Their Related Compounds. Ph.D. Dissertation, Michigan State University, East Lansing MI, 1989.

(26) Wernette, D. P.; Ichimura, A. S.; Urbin, S. A.; Dye, J. L. *Chem. Mater*. **2003**, *15*, 1441−1448.

(27) Dye, J. L.; Yemen, M. R.; DaGue, M. G.; Lehn, J.-M. *J. Chem. Phys.* **1978**, *68*, 1665−1670.

(28) Dye, J. L.; DaGue, M. G.; Yemen, M. R.; Landers, J. S.; Lewis, H. L. *J. Phys. Chem.* **1980**, *84*, 1096−1103.

(29) Redko, M. Y.; Jackson, J. E.; Huang, R. H.; Dye, J. L. *J. Am. Chem. Soc*. **2005**, *127*, 12416−12422.

(30) Hendrickson, J. E.; Pratt, W. P., Jr.; Phillips, R. C.; Dye, J. L. *J. Phys. Chem. B* **1998**, *102*, 3917−3926.

(31) Ichimura, A. S.; Wagner, M. J.; Dye, J. L. *J. Phys. Chem. B* **2002**, *106*, 11196−11202.

(32) Shin, D.-H.; Ellaboudy, A. S.; Dye, J. L.; DeBacker, M. G. *J. Phys. Chem.* **1991**, *95*, 7085−7089.

(33) (a) Werner, H.-J.; Knowles, P. J. *J. Chem. Phys.* **1985**, *82*, 5053. (b) Knowles, P. J.; Werner, H.-J. *Chem. Phys. Lett.* **1985**, *115*, 259.

(34) (a) For K: Bergner, A.; Dolg, M.; Kuechle, W.; Stoll, H.; Preuss, H. *Mol. Phys.* **1993**, *80*, 1431. (b) For Ca: Kaupp, M.; Schleyer, P. v. R.; Stoll, H.; Preuss, H. *J. Chem. Phys*. **1991**, *94*, 1360. (c) For Rf−Db: Dolg, M.; Stoll, H.; Preuss, H.; Pitzer, R. M. *J. Phys. Chem.* **1993**, *97*, 5852.